

Hard X-rays from Ultra-Compact H_{II} Regions in W49A

M. Tsujimoto¹, T. Hosokawa², E. D. Feigelson³, K. V. Getman³, & P. S. Broos³

ABSTRACT

We report the *Chandra* detection of hard X-ray emission from the Welch ring in W49A, an organized structure of ultra-compact (UC) H_{II} regions containing a dozen nascent early-type stars. Two UC H_{II} regions are associated with hard X-ray emission in a deep Advanced CCD Imaging Spectrometer image exposed for ~ 96.7 ks. One of the two X-ray sources has no near-infrared counterpart and is extended by $\sim 5''$, or ~ 0.3 pc, at a distance of ~ 11.4 kpc, which is spatially aligned with the cometary radio continuum emission associated with the UC H_{II} region. The X-ray spectrum of the emission, when fit with a thermal model, indicates a heavily absorbed plasma with extinction of $\sim 5 \times 10^{23}$ cm⁻², temperature ~ 7 keV, and X-ray luminosity in the 3.0–8.0 keV band of $\sim 3 \times 10^{33}$ ergs s⁻¹. Both the luminosity and the size of the emission resemble the extended hard emission found in UC H_{II} regions in Sagittarius B2, yet they are smaller by an order of magnitude than the emission found in massive star clusters such as NGC 3603 and the Arches cluster. Three possibilities are discussed for the cause of the hard extended emission in the Welch ring: an ensemble of unresolved point sources, shocked interacting winds of the young O stars, and a wind-blown bubble interacting with ambient cold matter.

Subject headings: stars: early-type — ISM: HII regions — ISM: individual (W49A, the Welch ring) — X-rays: ISM — radio continuum: ISM

1. INTRODUCTION

One of the interesting differences in X-ray-emitting phenomena between low-mass and high-mass star-forming regions is the existence of diffuse X-ray emission in high-mass regions. Extended emission in the soft X-ray band has been reported in some young massive clusters (e.g., M17 and the Rosette nebula; Townsley et al. 2003) and in nebulae surrounding Wolf-Rayet stars (e.g., S-308 and NGC 6888; Chu et al. 2003; Wrigge et al. 2005). Such emission is unlikely to arise from supernova remnants because these regions are expected to be too young to host supernova explosions. The X-ray spectrum can be explained by thermal plasma emission with a tempera-

ture of $\sim 10^6$ K and total luminosity of $\sim 10^{33}$ – 10^{34} ergs s⁻¹. In the latter two regions, soft X-rays are considered to be caused by a single Wolf-Rayet star, and hence the physical situation is simpler than the former two regions, which harbor a number of such massive objects.

The temperature, luminosity, and the physical scale of ~ 5 – 10 pc of the soft diffuse emission can be explained by the wind-blown bubble model, in which the fast winds from massive stars are thermalized by shocks colliding in the surrounding cold matter. Weaver et al. (1977) presented an analytical self-similar solution for this model, proposing that shock heating forms a bubble of hot gas that is observed as soft extended X-ray emission. The gas is contaminated by metals as a consequence of mass loss from massive stars, including main-sequence O-type stars and Wolf-Rayet stars. Such contamination has been observed as nitrogen-enriched chemical abundances in the optical spectra of some nebula (e.g., Esteban et al. 1992). In the soft diffuse emission from S-308, *XMM-Newton* measured elevated abundances con-

¹Department of Physics, Rikkyo University, 3-34-1, Nishi-Ikebukuro, Toshima, Tokyo 171-8501, Japan.

²National Astronomical Observatory of Japan, Osawa, Mitaka, Tokyo 181-8588, Japan.

³Department of Astronomy & Astrophysics, The Pennsylvania State University, 525 Davey Laboratory, University Park, PA 16802.

sistent with those reported for the cold surrounding nebula, supporting the wind-blown bubble model for the X-ray emission (Chu et al. 2003). The bubble model can be similarly applied to explain the diffuse X-ray emission around planetary nebulae (e.g., Dyson 1992; Kastner et al. 2001).

Much hotter extended emission has been reported by *Chandra* in other massive star-forming regions, including NGC 3603 (Moffat et al. 2002), the Arches and the Quintuplet clusters (Yusef-Zadeh et al. 2002; Law & Yusef-Zadeh 2004), Sagittarius B2 (Takagi et al. 2002), RCW 38 (Wolk et al. 2002), and NGC 6334 (Ezoe et al. 2006). The hard diffuse emission in these samples shows X-ray properties that differ from those of the soft diffuse X-ray emission. The typical plasma temperature is higher by more than an order of $\gtrsim 10^7$ K. The typical apparent size is much smaller of ~ 0.1 – 1 pc. Some of these hard spectra may be non-thermal (RCW 38 and NGC 6334; Wolk et al. 2002; Ezoe et al. 2006). Some show a strong fluorescent line from neutral or low-ionized iron at ~ 6.4 keV (Sagittarius B2, the Arches cluster; Takagi et al. 2002; Yusef-Zadeh et al. 2002), indicating that cold matter is involved in the process.

The origin of the hard extended emission is less clear. Cantó et al. (2000) presented an analytic model to describe the winds from a massive cluster interacting with each other and with the cold interstellar matter. Winds colliding with each other can give rise to a higher temperature in shock plasma than the winds colliding in the cold matter at rest. Takagi et al. (2002) speculated that the extended emission in Sagittarius B2 may be a collection of unresolved point sources comprising of both low-mass and high-mass members in the giant molecular cloud (GMC). Low-mass young stellar objects (YSOs) have been known as strong hard X-ray emitters due to flares caused by magnetic reconnection (Feigelson & Montmerle 1999). It has recently been proposed that magnetic activity may be responsible for the hard emission seen in some young O stars (Schulz et al. 2003; Gagné et al. 2005; Stelzer et al. 2005). There is also a possibility that the hard extended emission may be a special case of the wind-blown bubble employed to explain the soft diffuse emission. None of these explanations have conclusive observational evidence.

Such a phenomenon is particularly interesting

in ultra-compact (UC) H II regions. UC H II regions are ionized gas of a small size ($\lesssim 10^{17}$ cm) and a high density ($> 10^4$ cm $^{-3}$), which are associated with massive forming stars still embedded in their natal molecular clouds (Churchwell 2002). Two equally important energy sources governing the physics of UC H II regions are strong ultraviolet (UV) radiation and stellar winds from the forming massive stars (Capriotti & Kozminski 2001). The effect of the UV radiation, on one hand, is easier to assess, as the $\sim 10^4$ K plasma in equilibrium between the UV photo-ionization and the hydrogen recombination can be accessed using interferometers via centimeter continuum free-free emission, which penetrates through the extreme extinction ($A_V = 10^3$ – 10^4 mag) common among these regions. The effect of the stellar winds, on the other hand, is poorly constrained by observations and is often overlooked. If the hard extended emission is the outcome of such winds, it will provide a unique observational tool to investigate the wind effects, which will contribute to a complete understanding of the evolution and morphology of UC H II regions.

In this paper, we report the result of a deep hard X-ray study of a cluster of UC H II regions in W49A, known as the Welch ring. At a distance of ~ 11.4 kpc (Gwinn et al. 1992), W49A is one of the most active massive star-forming sites in our Galaxy (Alves & Homeier 2003). The total luminosity exceeds $\sim 10^7 L_\odot$. The Lyman continuum intensity of $\sim 10^{51}$ s $^{-1}$ is equivalent to ~ 100 O stars (Conti & Blum 2002). The Welch ring is the most curious object in the region, consisting of a dozen UC H II regions in an organized circular shape with a radius of ~ 1 pc (Welch et al. 1987). A dozen massive stars are being formed at the same time in a coherent structure. Numerous maser sources have been discovered (Gwinn et al. 1992; De Pree et al. 2000), indicating ongoing inflow and outflow motions. This structure is unique in our Galaxy and affords opportunities to seek insights into massive star formation and the interactions between massive stars and their environment. The present study is the first in the hard X-ray band.

2. OBSERVATIONS AND REDUCTION

An X-ray imaging-spectroscopy observation was conducted using ACIS (Advanced CCD Imaging Spectrometer; Garmire et al. 2003) on-board the *Chandra X-ray Observatory* (Weisskopf et al. 2002). The observation consists of two pointings, one for 33.5 ks (ObsID-5893) on 2005 August 3–4 and the other for 63.1 ks (ObsID-6355) on 2005 August 4–5. Both were planned with identical aim points (R. A. = $19^{\text{h}}12^{\text{m}}41^{\text{s}}.2$ and decl. = $09^{\text{d}}06^{\text{m}}51^{\text{s}}$) and roll angles, resulting in a combined data set that covers a $\sim 17' \times 17'$ field for a total integration time of ~ 96.7 ks. ACIS is sensitive in the 0.5–8.0 keV energy band with an energy resolution of ~ 150 eV at 6 keV. The size of the point spread function (PSF), represented by the 90% encircled energy radius of a point source, is ~ 1 and $\sim 2''$ for 1.5 and 6 keV photons within $2'$ around the optical axis. The faintest detected source has a flux of $\sim 10^{-15.3}$ ergs $\text{s}^{-1} \text{cm}^{-2}$ (0.5–8.0 keV). The detector was operated with the Timed Exposure mode with the nominal frame time. We used the Very Faint telemetry mode to remove background events based on 5×5 pixel charge distributions.

Figure 1a shows a pseudo-color smoothed image of the ACIS field. The bright extended structure at the eastern edge of the field is the supernova remnant W49B, which is unrelated to W49A. Figure 1b shows a closer view of the major massive star clusters, including W49A South, the Welch ring, O3, S, and Q. Near-infrared (NIR) sources associated with the clusters W49A South, O3, S, and Q have colors redder than $(H-K_S) = 2$ mag due to a visual extinction of ~ 32 mag (Alves & Homeier 2003), corresponding to a hydrogen-equivalent column density of $\sim 5.7 \times 10^{22} \text{ cm}^{-2}$ assuming a standard dust-to-gas ratio (Predehl & Schmitt 1995). Some X-ray photons are detected through this heavy extinction.

We used the CIAO package for the source detection and the ACIS Extract¹ software package for the systematic analysis of X-ray photometry, variability, and spectroscopy. The details of the procedure are described in Getman et al. (2005).

¹The ACIS Extract software and User's Guide have been available online at http://www.astro.psu.edu/xray/docs/TARA/ae_users_guide.html since February 2003.

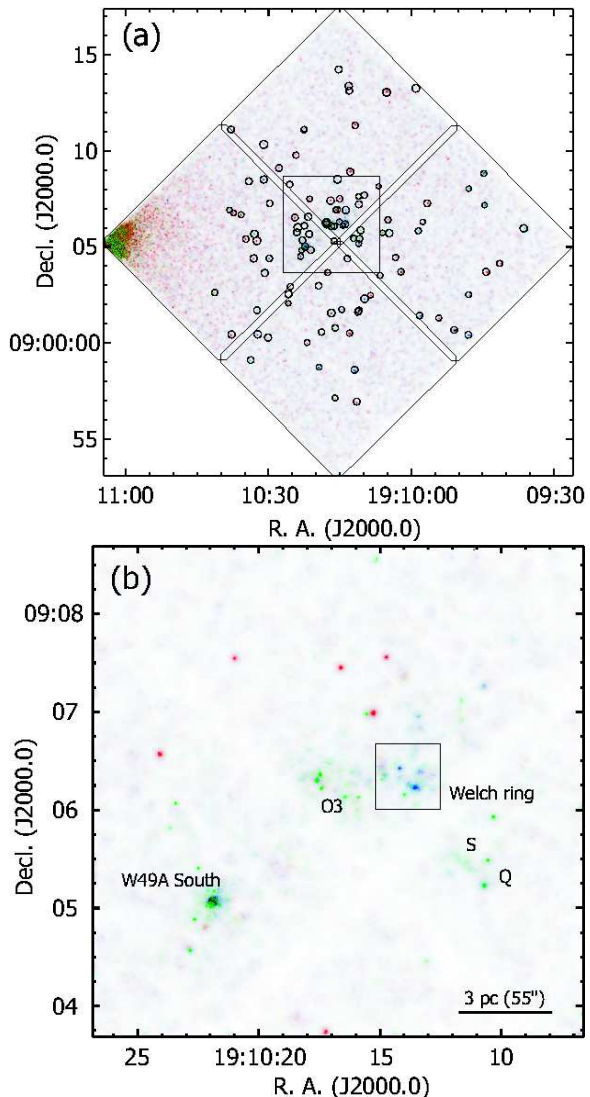


Fig. 1.— (a) Pseudo-color smoothed image of the ACIS field. The views of the four CCD chips are shown with the oblique squares. Circles indicate the positions of detected X-ray sources. Red, green, and blue indicate the intensity in the 0.5–2.3 (soft), 2.3–4.3 (medium), and 4.3–8.0 keV (hard) bands, respectively. The energy bands are chosen so that each band contains roughly equal numbers of photons. (b) Close-up view of W49A (the central square in a). The color coding is the same as (a). The figure can be compared to Figure 1 in Alves & Homeier (2003) with the same dimension. An expanded view of the Welch ring region (the square in panel b) is shown in Figure 2.

In total, 107 X-ray sources were detected. The position of these sources are plotted in Figure 1 (a). We concentrate on the hard X-ray emission associated with the Welch ring in this paper. The X-ray properties of the other sources will be presented separately. The astrometric uncertainty of the X-ray sources is $\sim 0''.35$ estimated using 21 pairs of ACIS and Two Micron All Sky Survey (2MASS; Cutri et al. 2001) counterparts.

3. ANALYSIS

3.1. X-ray Sources in the Welch Ring

Figure 2 shows a multi-wavelength pseudo-color smoothed image of the Welch ring using X-ray, NIR, and radio continuum observations with blue, green, and red colors, respectively. The ring can be best traced by the radio continuum image in red; a dozen UC H II regions labeled from A through M shape an ellipse of $\sim 30'' \times 12''$ in major and minor axes and $\sim 60^\circ$ in position angle. The nomenclatures follow De Pree et al. (1997).

Conti & Blum (2002) and Alves & Homeier (2003) reported NIR detections from two of the UC H II regions (F and J2) identified by centimeter observations (Dreher et al. 1984; De Pree et al. 1997). Other NIR sources in Figure 2 are likely to be foreground stars because of their blue colors in the J -, H -, and K_S -band photometry using the 2MASS data.

Among the UC H II regions in the Welch ring, two are associated with X-ray emission (F and G; Fig. 2). From their positional coincidence, we consider that these two X-ray sources are physically related to the UC H II regions F and G. The X-ray source at F is consistent with a point source, while that at G appears extended. This source is the main subject of this paper; we designate it CXOU J191013.5+090612, hereafter abbreviated to source G_X .

3.2. X-ray Image and Spectrum of G_X

Figure 3 shows the spectrum of the source G_X extracted from the aperture shown by the polygon in Figure 2). For technical reasons, it was convenient to make the aperture a contour of the PSF that would enclose 99% of a point-like source, which is large enough to cover the extended emission of G_X . The extracted events consist of 101

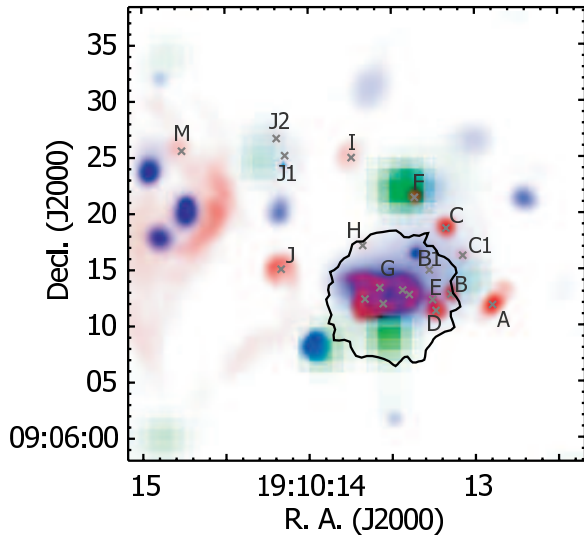


Fig. 2.— Multi-wavelength pseudo-color smoothed image of the Welch ring. Red, green, and blue indicate the intensity in the 3.6 cm (De Pree et al. 2000), NIR K_S (2MASS; Cutri et al. 2001), and the X-ray (0.5–8.0 keV) bands, respectively. Crosses indicate the positions of the 3.6 cm sources labeled with their names (De Pree et al. 1997). The complex of objects named G1–G5 are labeled “G”. The solid polygon is the extraction region of the X-ray events associated with the source G.

counts with an estimated local background of ~ 18 counts. No flux variability was confirmed with the null hypothesis (constant flux) probability of 0.37. The spectrum was binned to 10 counts bin^{-1} and was fit over the energy range of 3.0–8.0 keV. The spectrum is strongly cutoff at the softer end but is extremely hard such that the count rate hardly falls despite the rapidly falling sensitivity of ACIS above ~ 5 keV. This is very unusual, indicating an extremely hard intrinsic spectrum that cannot be attributed to heavy absorption. The median energy of source is 5.7 keV, which is matched by only 2 of the 1616 sources in the deep X-ray census of the Orion Nebula region (Getman et al. 2005). Both thermal and non-thermal models were tried for fitting since the data are not sufficient to detect or reject iron emission lines, which would otherwise constrain the spectral models.

First, a thin-thermal-plasma APEC model (Smith et al. 2001) with interstellar extinction was applied. The metallicity was fixed to 0.3 solar following the convention in Getman et al. (2005). The minimum χ^2 value was obtained for a hydrogen-equivalent column density of $N_{\text{H}} = 5.1^{+2.5}_{-1.8} \times 10^{23} \text{ cm}^{-2}$ and a plasma temperature of $k_{\text{B}}T \sim 7$ keV. The fit is statistically acceptable, corresponding to a null hypothesis probability for the χ^2 value of 0.23. The uncertainties quoted for the N_{H} value indicate the 90% confidence interval. No meaningful confidence interval was available for $k_{\text{B}}T$ because of the relatively poor spectrum. Values of χ^2 were calculated at 10^4 different sets of parameters in the range of $N_{\text{H}} = 0\text{--}100 \times 10^{22} \text{ cm}^{-2}$ and $k_{\text{B}}T = 0.5\text{--}20$ keV, but no other local minimum was found. The flux in the 3.0–8.0 keV is $\sim 4 \times 10^{-14} \text{ ergs s}^{-1} \text{ cm}^{-2}$, and the absorption-corrected luminosity in the band is $\sim 3 \times 10^{33} \text{ ergs s}^{-1}$.

Second, a power-law model of $E^{-\Gamma}$ with interstellar extinction was applied. The minimum χ^2 value was obtained for $N_{\text{H}} \sim 2.1 \times 10^{22} \text{ cm}^{-2}$ and $\Gamma \sim -2.7$. No other local minimum was found in the $(N_{\text{H}}\text{--}\Gamma)$ plane. The fit is statistically acceptable, but the positive power-law slope is unphysical. Therefore, we hereafter refer to the results of the thermal fit.

In order to examine the extent of the source G_{X} in comparison with the PSF, we plot the radial profile of this source (Fig. 4). A comparison source (CXOU J191010.4+090528) at a similar off-

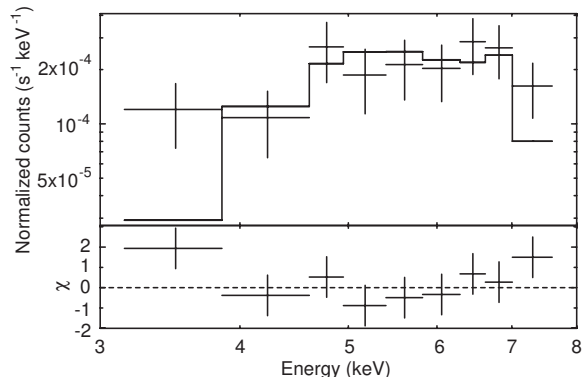


Fig. 3.— X-ray spectrum of the source G_{X} . Grouped data with errors are shown in the upper panel over-plotted with the best-fit plasma model convolved with mirror and detector responses (*solid line*). The lower panel shows the residuals of the fit.

axis angle with a similar median X-ray energy is also plotted. G_{X} and the comparison source are located at off-axis angles of $1'.6$ and $1'.8$ and have median energies of 5.7 and 4.1 keV, respectively. We find that G_{X} is extended with a radius of $\sim 5''$ (~ 0.3 pc) in contrast to the point-like comparison source, which has a profile consistent with the PSF at its position.

3.3. Source G in Other Wavelengths

In the region around G_{X} , De Pree et al. (1997) detected five sources (G1–5) using the Very Large Array (VLA) in its shorter baseline configurations (C and D) at 3.6, 1.3, and 0.7 cm. De Pree et al. (2000) subsequently detected G1 and resolved G2 into three compact sources (G2a–c) using VLA in the longer baseline configurations (A and B) at 1.3 and 0.7 cm. BIMA observations also detected the four compact sources (G1 and G2a–c) at 3.3 mm (De Pree et al. 2000) and 1.4 mm (Wilner et al. 2001) with a similar synthesized beam width ($0'.1\text{--}0'.3$). These compact sources are presumably newly formed massive stars. In contrast, the lack of detection of G3–5 by the higher resolution interferometer observations indicates that these sources are parts of a cometary structure, as is discussed in De Pree et al. (2000), extending $\sim 4''$ eastward of G1 and G2, shown as contours in Fig. 5. (See also see Fig. 1 in Dreher et al. 1984 and Fig. 1 in De Pree et al. 2000). The nature of the cometary

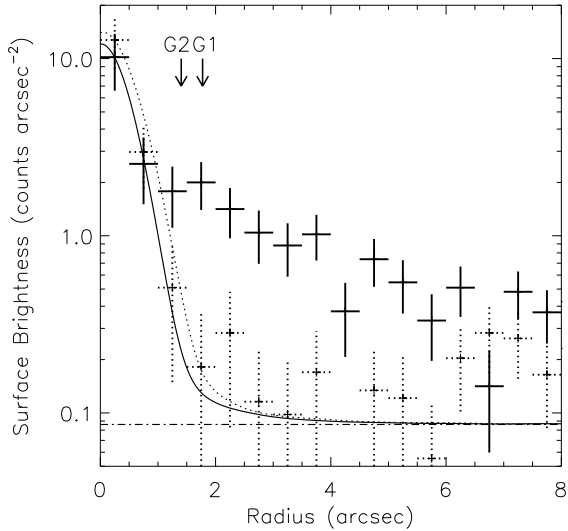


Fig. 4.— Observed radial profiles of the source G_X (solid pluses) and the comparison source CXOU J191010.4+090528 (dotted pluses). The radial profiles of the local model PSFs (solid and dotted curves) are shown, elevated on the observed background (dashed-and-dotted line). The displacements from the center of G_X to the closest radio compact sources (G1 and G2; De Pree et al. 1997) are shown by arrows.

emission is uncertain.

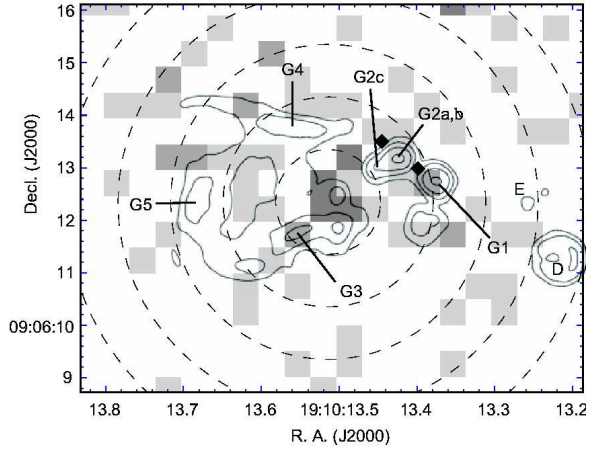


Fig. 5.— X-ray intensity map of the source G_X in grey scale (from 0 to 3 counts pixel $^{-1}$). The contours are 1.3 cm intensity (Fig. 1c in De Pree et al. 2000) with the names of radio compact sources (G1, G2a, and G2b) and knots in a lobe-like extended structure (G3–5). The concentric circles indicate the distance from the peak of the X-ray emission in 1'' steps. The diamonds show the position of two additional peaks in the deconvolved X-ray image.

In the infrared regime, the extreme extinction to this source prevents access by NIR (Conti & Blum 2002; Alves & Homeier 2003) and mid-infrared (MIR; Smith et al. 2000) observations shortward of 12.3 μm . In the 20.6 μm image, a source appears at G, showing an extended structure with a scale of $\sim 5''$ attributable to thermal emission from heated dust grains (Smith et al. 2000).

The peak of the X-ray emission does not coincide with the positions of any compact sources in the radio continuum (G1 and G2; Figs. 4 and 5), which are displaced from the X-ray peak by $\gtrsim 1''.5$ (Fig. 4). We constructed an X-ray image deconvolved with the PSF using a maximum likelihood reconstruction technique (Lucy 1974). Deconvolved images often introduce artificial peaks, and the only practical way to examine the validity of these new peaks is to see whether they match the sources detected in higher resolution images in other wavelengths. In the deconvolved X-ray image around G_X , we found two peaks at the positions shown with the diamonds in Figure 5. The locations of these peaks near the positions of G1

and G2 suggest X-ray emission from these sources, especially if an astrometric misalignment of $\sim 0''.4$ is allowed. A deeper observation will be required to confirm emission from G1 and G2. However, there is no question that most of the hard X-ray emission from G_X arises from a region displaced 1–2'' eastward of G1 and G2. No more than 10% of the counts are from G1 and G2.

4. DISCUSSION

4.1. Comparison with Other Hard Extended Emission

We can summarize the X-ray properties associated with the UC H II region G in the Welch ring as follows. It has a luminosity of $\sim 3 \times 10^{33}$ ergs s^{-1} and its spectrum can be fitted with thermal plasma of a temperature of ~ 7 keV and an interstellar extinction of $\sim 5 \times 10^{23}$ cm^{-2} . The profile is extended and a size of ~ 0.3 pc. The center of the diffuse emission is offset from the closest compact radio sources.

These findings can be compared with the properties of the hard diffuse emission previously claimed in other regions, listed in Table 1 in increasing order of distance. The parameters of the diffuse emission in the Quintuplet cluster were not constrained very well because the emission is overwhelmed by the intense diffuse emission in the Galactic center (Law & Yusef-Zadeh 2004). The numbers in Table 1 cannot be compared naively because of the different reduction techniques used by different authors. However, the X-ray properties of G_X resemble those found for UC H II regions in Sagittarius B2, in terms of the X-ray luminosity, the temperature, the amount of extinction, and the size. Both the X-ray luminosity and the size of these sources are smaller by an order of magnitude than those found in star clusters like NGC 3603, Arches, and Quintuplet. It thus appears that there are two categories for the hard diffuse emission from the view point of the X-ray luminosity and the size.

Based on the results in the Welch ring and the comparison with the other regions, we explore the three possible causes outlined in §1: a collection of unresolved point sources, interacting O star winds, and a wind-blown bubble.

4.2. Population of Point Sources

The first possibility for the cause of the diffuse emission at G is that it is a collection of unresolved point sources. As the region contains forming early-type stars, it should also contain numerous low-mass YSOs born from the same molecular cloud. Because both low-mass YSOs and massive young stars show hard X-ray emission, the collection of these sources can mimic hard diffuse emission when they are unresolved. The total X-ray emission from these sources can be estimated in the following manner.

First, the number of massive stars in this region is inferred using two indirect methods; any direct census of massive stars is difficult due to the extreme extinction that prevents observations of photospheric emission from these stars in the optical and NIR bands. One method is to use the luminosity of dust emission warmed by massive stars in the MIR band. Smith et al. (2000) found that the integrated luminosity between 12 and 20 μm is $\sim 2 \times 10^5 L_\odot$, which corresponds to a single zero-age main-sequence (ZAMS) star of spectral type O6. Another method is to use the Lyman continuum photons emitted per unit time derived from the radio continuum flux. De Pree et al. (2000) estimate that two O5.5 ZAMS stars are present. These two independent estimates both indicate there are 1–2 O5–6 ZAMS sources in region G.

We scale the estimate of high-mass population in G_X to the X-ray luminosity function of the Orion Nebula Cluster (ONC), the star-forming region best studied by *Chandra* (Getman et al. 2005). In the ONC, one O6 V star (θ^1 Ori C) accounts for one third of the total hard emission, while the whole of the lower mass (0.3–3.0 M_\odot) YSO population accounts for one half (Feigelson et al. 2005). In G_X , where 1–2 O5–6 sources are present, we estimate that the total hard X-ray luminosity of point sources is ~ 1 – 2×10^{33} ergs s^{-1} , which is on the same order as the observed luminosity.

In NGC 3603 and NGC 6334, Moffat et al. (2002) and Ezoe et al. (2006) respectively estimated that $\sim 25\%$ and $\sim 20\%$ of the diffuse flux can be explained by unresolved faint point sources based on the X-ray luminosity function constructed in each region. In the Welch ring, on the other hand, we cannot construct the luminos-

TABLE 1
HARD DIFFUSE X-RAY EMISSION FROM HIGH-MASS STAR-FORMING REGIONS.

Region	L_X^a (ergs s $^{-1}$)	$k_B T^b$ (keV)	N_H^c (cm $^{-2}$)	Size d (pc)	Distance (kpc)	Comment	Reference
RCW 38	1×10^{32}	2.2	1×10^{22}	1.5	1.7	cluster	Wolk et al. (2002)
NGC 6334	$0.1\text{--}5 \times 10^{32}$	>1	$0.5\text{--}10 \times 10^{22}$	1	1.7	GMC	Ezoe et al. (2006)
NGC 3603	2×10^{34}	3.1	7×10^{21}	4	7.0	cluster	Moffat et al. (2002)
Arches	2×10^{34}	5.7	1×10^{23}	3	8.5	cluster	Yusef-Zadeh et al. (2002)
Quintuplet	1×10^{34}	8.5	cluster	Law & Yusef-Zadeh (2004)
Sgr B2 source 10	9×10^{32}	10	4×10^{23}	0.2	8.5	UC H II	Takagi et al. (2002)
Sgr B2 source 13	1×10^{33}	5	4×10^{23}	0.2	8.5	UC H II	Takagi et al. (2002)
W49A G $_X$	3×10^{33}	7	5×10^{23}	0.3	11.4	UC H II	this work

^aAbsorption-corrected X-ray luminosity.

^bPlasma temperature.

^cInterstellar extinction.

^dPhysical size of the diffuse emission.

ity function specific to this region. Considering this ambiguity, it is possible that all of the X-ray flux from G $_X$ can be attributed to the integrated emission of unresolved point sources.

4.3. Interacting Winds

In massive star clusters, winds from each massive star collide to produce shock-heated plasma (Ozernoy et al. 1997). This is a favored model to explain the extended hard X-ray emission based on the fact that it is easier to produce hard X-ray emission because it can produce higher temperature plasma than the bubble model (§4.4). In the Welch ring, the interacting winds could naturally explain the fact that similar extended X-ray emission is not found in other UC H II regions at the same level; G is the only region that was resolved into several bright compact radio continuum sources (De Pree et al. 2000), indicating the existence of multiple early-type stars. Numerical models have been developed to explain the diffuse emission associated with the Arches cluster (Raga et al. 2001; Cantó et al. 2000; Rockefeller et al. 2005). A similar model could be developed for the Welch ring emission for quantitative comparison.

A related possibility is the production of hard X-rays from small-scale wind shocks in Wolf-Rayet binary systems. Here, the X-ray luminosity reaches $\sim 10^{33}$ erg s $^{-1}$ and temperatures as high as $\sim 10^8$ K (e.g., Pollock 1987; Usov 1992). Most of the observed flux should arise from the position

where the two winds collide head-on to produce a peak temperature plasma; plasma in the periphery is subject to cooling as discussed in the next subsection. The observed luminosity and temperature of G $_X$ are similar to those observed in Wolf-Rayet binary systems. Therefore, the X-ray emission in G can also be explained by the colliding winds from multiple forming massive stars.

4.4. Wind-blown Bubble

A wind-blown bubble model has been employed to explain the soft diffuse emission in other regions (Townsend et al. 2003; Chu et al. 2003; Wrigge et al. 2005). The application of this model to G $_X$ is inspired by the fact that G, unlike other UC H II regions in the Welch ring, is also associated with lobe-like extended radio emission with the same scale around the diffuse X-ray emission. The bubble model has also been used to explain the coherent space velocities of water maser sources from the very source of G (Mac Low & Elitzur 1992), where it was proposed that these sources are from the expanding shells swept by stellar winds. The involvement of cold matter in the hard X-ray emission is strongly inferred by the detection of the fluorescent iron line in Sagittarius B2 and the Arches cluster (Takagi et al. 2002; Yusef-Zadeh et al. 2002). Because this possibility for the X-ray emission has not been discussed in previous works, we examine this idea here in more detail.

Wind-blown bubbles are formed as a conse-

quence of strong stellar winds from massive stars and have been modeled in various circumstances. A classic study of Weaver et al. (1977) discusses a case in which the strong wind collides with the uniform cold interstellar medium of a $\sim 1 \text{ cm}^{-3}$ density. They argued that the bubble is filled with hot ($T > 10^6 \text{ K}$) gas by shocks of stellar wind and the swept-up medium forms a spherical shell.

Analogous to Figure 1 in Weaver et al. (1977), we consider the case in which the winds from massive stars impinge on ambient $\sim 10^4 \text{ K}$ gas ionized in advance by UV photons. In the initial stage, the ionization front travels at a much faster speed than the winds (a typical wind velocity is $\sim 2000 \text{ km s}^{-1}$ for main sequence O-type stars; Lamers & Leitherer 1993). Figure 6 shows four layers in a quadrant of the spherically symmetric model: (a) pre-shock stellar wind, (b) shocked stellar wind, (c) shocked $\sim 10^4 \text{ K}$ gas, and (d) pre-shock $\sim 10^4 \text{ K}$ gas. The reverse shock (RS) and the contact discontinuity (CD) mark the (a)–(b) and (b)–(c) boundaries, respectively. The four-layer structure is discussed by numerous authors besides Weaver et al. (1977). Note the assumption that the fast wind collides in ionized gas, not in cold matter. Such a situation is also developed by Capriotti & Kozminski (2001) for H II regions and by Frank & Mellema (1994) for planetary nebulae, where both photo-ionization and winds are important.

This configuration can be applied to the observational results in the following way. The compact radio sources (G1 and G2) are forming massive stars at the center, the extended X-ray emission (G_X) is from region (b), and the cometary extended radio emission is mainly from region (c). The density is higher in region (c) than in region (d) after experiencing a shock, and the radio emission measure is proportional to the square of the density. It is hardly possible that the UV photo-ionized plasma emits detectable emission in the hard X-ray band. We therefore consider that two plasmas of different origins coexist in a system; one being the wind-shocked $\sim 10^8 \text{ K}$ gas responsible for the diffuse X-ray emission and the other being the UV photo-ionized $\sim 10^4 \text{ K}$ gas responsible for the diffuse radio continuum emission.

In order to examine the validity of this picture, we can roughly quantify the model for the G_X conditions. First, the shock temperature in the adi-

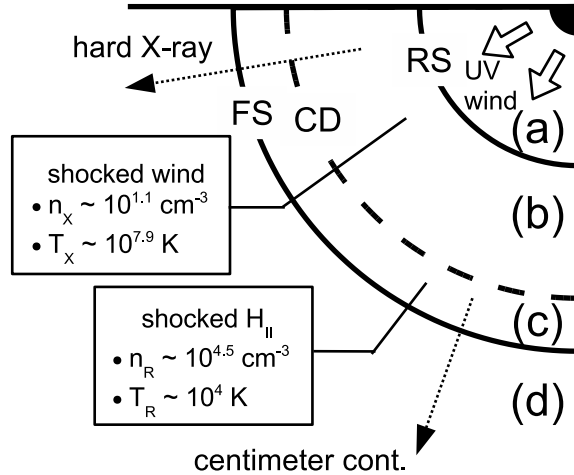


Fig. 6.— Schematic view of the wind-blown bubble caused by winds colliding with $\sim 10^4 \text{ K}$ gas ionized in advance by UV photons around a young massive star. The pre-shock stellar wind (a), shocked stellar wind (b), shocked 10^4 K gas (c), and pre-shock 10^4 K gas (d) are separated by the reverse shock (RS), the contact discontinuity (CD), and the forward shock (FS), respectively.

abatic case of $(3\mu m_H)/(16k_B)v_w^2 \sim 5 \text{ keV}$ is consistent with the observed value of $\sim 7 \text{ keV}$, where m_H is the hydrogen mass, $\mu \sim 0.6$ is the average particle mass relative to hydrogen, and $v_w \sim 2000 \text{ km s}^{-1}$ is the wind velocity inferred to account for the maser emission (Mac Low & Elitzur 1992). Second, if the observed X-ray and radio emission arise respectively from regions (b) and (c), then the pressures of these plasmas are expected to be equal, since the pressure is constant across the contact discontinuity. The pressure inside the discontinuity is $n_X k_B T_X \sim 1 \times 10^{-7} \text{ dyn cm}^{-2}$, where T_X is the observed X-ray temperature and $n_X = \sqrt{(EM_X/V_X)} \sim 1 \times 10^1 \text{ cm}^{-3}$ is the gas density derived from the observed X-ray emission measure EM_X and the assumption that the gas fills a spherical volume of a radius of 0.3 pc. Similarly, the pressure outside the discontinuity is estimated from the radio data as $n_R k_B T_R = 4 \times 10^{-8} \text{ dyn cm}^{-2}$, where $T_R \sim 10^4 \text{ K}$ is the assumed photo-ionized gas temperature and $n_R \sim 3 \times 10^4 \text{ cm}^{-3}$ is its density. The density value was derived for sources G3–5 in the shorter baseline VLA observations (De Pree et al. 1997) and

is assumed to represent the value of the radio cometary structure, which we associate with region (c). The pressures across the contact discontinuity thus agree within a factor of a few.

The main problem in applying the bubble model is the difficulty in attaining the observed high plasma temperature of ~ 80 MK. Although the adiabatic shock temperature is high enough to explain the observed value, the conduction may quickly cool the plasma down to $\sim 10^6$ – 10^7 K by interaction with cold matter. Note here that the radiative cooling does not play an important role because the cooling time of $(3n_X k_B T_X)/(1.4 \times 10^{-27} \sqrt{T_X} n_X^2 \bar{g}_{\text{ff}}) \sim 5 \times 10^6$ yr is longer than the suggested lifetime of the system ($\sim 10^3$ yr; Mac Low & Elitzur 1992), where $\bar{g}_{\text{ff}} \sim 1.2$ is the average Gaunt factor of the free-free emission. The suppression of the conduction rate by magnetic fields wrapping the bubble needs to be considered for this model as in cluster of galaxies and supernova remnants (e.g., Malyshkin 2001; Velázquez et al. 2004). González-Avilés et al. (2005) calculated the bubble temperature for different conduction rates (κ/κ_c , where κ_c is the classical value) and found that the temperature under a conduction rate of $\kappa/\kappa_c < 1/5$ is lower than that under the adiabatic case ($\kappa/\kappa_c = 0$) by only a factor of a few. Under such conditions, the wind-blown bubble model can probably account for the observed high plasma temperature.

5. SUMMARY

We study the Welch ring in W49A in the hard X-ray band for the first time using the *Chandra X-ray Observatory*. An extended source with a radius of $\sim 5''$ (~ 0.3 pc) was found to be associated with one of the UC H II regions (G) in the ring. It has a X-ray luminosity of $\sim 3 \times 10^{33}$ ergs s $^{-1}$ (3.0–8.0 keV) with a spectrum fit by a thermal plasma at a temperature of ~ 7 keV and an interstellar extinction of $\sim 5 \times 10^{23}$ cm $^{-2}$. The source is extended to a scale similar to a lobe-like structure in the radio continuum. The center of the diffuse X-ray emission is offset from the closest compact radio sources. The observed properties are similar to those found for the X-ray emission in the UC H II regions in Sagittarius B2.

Three possibilities are discussed for the cause

of the hard emission. The ensemble of unresolved hard point sources from lower mass YSOs associated with the O stars can explain both the observed X-ray luminosity and temperature of the extended emission. Interacting winds from multiple massive stars can also explain the observed properties. This idea also naturally explains why similar hard extended emission is not found in other UC H II regions in the Welch ring, where G is the only complex resolved into several bright compact radio sources. A wind-blown bubble may be able to explain the extended X-ray and radio emission at the same time, but it requires that conductive cooling is significantly suppressed across the contact surface. From the available data, we cannot conclusively choose one model for the emission in the Welch ring over the others, and the production mechanism of the hard diffuse emission remains an open question.

The authors express gratitude to Chris De Pree for sharing his radio continuum images. M. T. acknowledges financial support by the Japan Society for the Promotion of Science and the *Chandra* guest observer grant. E.D.F., K.V.G. and P.S.B. are supported by *Chandra* Contract SV4-74018 (G. Garmire, PI) issued by the *Chandra* X-ray Observatory Center, which is operated by the Smithsonian Astrophysical Observatory for and on behalf of NASA under contract NAS8-03060. This publication uses data products from the Two Micron All Sky Survey, which is a joint project of the University of Massachusetts and the Infrared Processing and Analysis Center/California Institute of Technology, funded by the National Aeronautics and Space Administration and the National Science Foundation.

Facilities: CXO(ACIS)

REFERENCES

- Alves, J., & Homeier, N. 2003, *ApJ*, 589, L45
- Cantó, J., Raga, A. C., & Rodríguez, L. F. 2000, *ApJ*, 536, 896
- Capriotti, E. R., & Kozminski, J. F. 2001, *PASP*, 113, 677
- Chu, Y.-H., Guerrero, M. A., Gruendl, R. A., García-Segura, G., & Wendker, H. J. 2003, *ApJ*, 599, 1189

- Churchwell, E. 2002, *ARA&A*, 40, 27
- Conti, P. S., & Blum, R. D. 2002, *ApJ*, 564, 827
- Cutri, R. M., et al. 2001, *Astronomical Society of the Pacific Conference Series*, 232, 78
- De Pree, C. G., Mehringer, D. M., & Goss, W. M. 1997, *ApJ*, 482, 307
- De Pree, C. G., Wilner, D. J., Goss, W. M., Welch, W. J., & McGrath, E. 2000, *ApJ*, 540, 308
- Dreher, J. W., Johnston, K. J., Welch, W. J., & Walker, R. C. 1984, *ApJ*, 283, 632
- Dyson, J. E. 1992, *MNRAS*, 255, 460
- Esteban, C., Vilchez, J. M., Smith, L. J., & Clegg, R. E. S. 1992, *A&A*, 259, 629
- Ezoe, Y., Kokubun, M., Makishima, K., Sekimoto, Y., & Matsuzaki, K. 2006, *ApJ*, 638, 860
- Feigelson, E. D., & Montmerle, T. 1999, *ARA&A*, 37, 363
- Feigelson, E. D., et al. 2005, *ApJS*, 160, 379
- Frank, A., & Mellema, G. 1994, *A&A*, 289, 937
- Gagné, M., Oksala, M. E., Cohen, D. H., Tonnesen, S. K., ud-Doula, A., Owocki, S. P., Townsend, R. H. D., & MacFarlane, J. J. 2005, *ApJ*, 628, 986
- Garmire, G. P., Bautz, M. W., Ford, P. G., Nousek, J. A., & Ricker, G. R. 2003, *Proc. SPIE*, 4851, 28
- Getman, K. V., et al. 2005, *ApJS*, 160, 319
- González-Avilés, M., Lizano, S., & Raga, A. C. 2005, *ApJ*, 621, 359
- Gwinn, C. R., Moran, J. M., & Reid, M. J. 1992, *ApJ*, 393, 149
- Kastner, J. H., Vrtilik, S. D., & Soker, N. 2001, *ApJ*, 550, L189
- Lamers, H. J. G. L. M., & Leitherer, C. 1993, *ApJ*, 412, 771
- Law, C., & Yusef-Zadeh, F. 2004, *ApJ*, 611, 858
- Lucy, L. B. 1974, *AJ*, 79, 745
- Mac Low, M.-M., & Elitzur, M. 1992, *ApJ*, 393, L33
- Malyszhkin, L. 2001, *ApJ*, 554, 561
- Moffat, A. F. J., et al. 2002, *ApJ*, 573, 191
- Ozernoy, L. M., Genzel, R., & Usov, V. V. 1997, *MNRAS*, 288, 237
- Pollock, A. M. T. 1987, *ApJ*, 320, 283
- Predehl, P., & Schmitt, J. H. M. M. 1995, *A&A*, 293, 889
- Raga, A. C., Velázquez, P. F., Cantó, J., Masciadri, E., & Rodríguez, L. F. 2001, *ApJ*, 559, L33
- Rockefeller, G., Fryer, C. L., Melia, F., & Wang, Q. D. 2005, *ApJ*, 623, 171
- Schulz, N. S., Canizares, C., Huenemoerder, D., & Tibbets, K. 2003, *ApJ*, 595, 365
- Smith, N., et al. 2000, *ApJ*, 540, 316
- Smith, R. K., Brickhouse, N. S., Liedahl, D. A., & Raymond, J. C. 2001, *ApJ*, 556, L91
- Stelzer, B., Flaccomio, E., Montmerle, T., Micela, G., Sciortino, S., Favata, F., Preibisch, T., & Feigelson, E. D. 2005, *ApJS*, 160, 557
- Takagi, S., Murakami, H., & Koyama, K. 2002, *ApJ*, 573, 275
- Townsley, L. K., Feigelson, E. D., Montmerle, T., Broos, P. S., Chu, Y.-H., & Garmire, G. P. 2003, *ApJ*, 593, 874
- Usov, V. V. 1992, *ApJ*, 389, 635
- Yusef-Zadeh, F., Law, C., Wardle, M., Wang, Q. D., Fruscione, A., Lang, C. C., & Cotera, A. 2002, *ApJ*, 570, 665
- Velázquez, P. F., Martinell, J. J., Raga, A. C., & Giacani, E. B. 2004, *ApJ*, 601, 885
- Weaver, R., McCray, R., Castor, J., Shapiro, P., & Moore, R. 1977, *ApJ*, 218, 377
- Weisskopf, M. C., Brinkman, B., Canizares, C., Garmire, G., Murray, S., & Van Speybroeck, L. P. 2002, *PASP*, 114, 1

Welch, W. J., Dreher, J. W., Jackson, J. M., Terebey, S., & Vogel, S. N. 1987, *Science*, 238, 1550

Wilner, D. J., De Pree, C. G., Welch, W. J., & Goss, W. M. 2001, *ApJ*, 550, L81

Wolk, S. J., Bourke, T. L., Smith, R. K., Spitzbart, B., & Alves, J. 2002, *ApJ*, 580, L161

Wrigge, M., Chu, Y.-H., Magnier, E. A., & Wendker, H. J. 2005, *ApJ*, 633, 248